

Supporting Text - Jégou et al.

I. PAUSES DURING DEPOLYMERIZATION

Pauses were observed during the depolymerization of individual filaments grown from ADP-, CrATP- or MgATP-actin, in the presence or in the absence of profilin. As discussed in the main text, these pauses did not affect the depolymerization traces up to the interruption. Moreover, as can be seen from Fig. S1 and Fig. S2, the occurrence of a pause did not affect the depolymerization velocity for segments depolymerizing before or after the pause. The mechanism underlying the pausing events will be elucidated elsewhere [T. Niedermayer, A. Jégou, E. Helfer, G. Romet-Lemonne, M.-F. Carlier, R. Lipowsky, *in preparation*].

II. THEORETICAL ANALYSIS

We analyze the filament disassembly which is controlled by the dynamics of the nucleotide state of the actin subunit at the barbed end. As discussed in the main text, ATP is quickly cleaved, so we may only consider ADP-Pi-actin and ADP-actin subunits, respectively. This simplification is validated by the simulations described in section IV.

A. Random phosphate release

We consider the average depolymerization velocity of an ensemble of N filaments

$$v_{\text{depol}}(t) \equiv \frac{1}{N} \sum_{i=1}^N v_{\text{depol}}^i(t), \quad (1)$$

where the individual depolymerization velocities $v_{\text{depol}}^i(t)$ are solely determined by the state of the subunit at the barbed end of the i -th filament. As discussed in the main text, an ADP-Pi-subunit can either dissociate directly with the rate $k_{\text{off}}^{\text{ADP-Pi}}$, or first release its phosphate with the rate k_{r}^{BE} and then dissociate as an ADP-subunit with the rate $k_{\text{off}}^{\text{ADP}}$, see fig. 3 in the main text. In our experiments, we do not distinguish between these two routes. Thus we define an effective ADP-Pi-actin depolymerization rate $v_{\text{depol}}^{\text{ADP-Pi}}$ as the inverse of the mean time that it takes for an ADP-Pi-subunit to depart from the barbed end. It can be computed considering the following. The fraction $k_{\text{off}}^{\text{ADP-Pi}}/(k_{\text{r}}^{\text{BE}} + k_{\text{off}}^{\text{ADP-Pi}})$ of the ADP-Pi-subunits at the barbed end dissociate directly, while the fraction $k_{\text{r}}^{\text{BE}}/(k_{\text{r}}^{\text{BE}} + k_{\text{off}}^{\text{ADP-Pi}})$ first releases its phosphate before dissociating as ADP-actin. The dwell time of the initial ADP-Pi-state is given by $1/(k_{\text{r}}^{\text{BE}} + k_{\text{off}}^{\text{ADP-Pi}})$, and the dwell time of the ADP-state is given by $1/k_{\text{off}}^{\text{ADP}}$. In consequence, the

combination of the two routes leads to

$$v_{\text{depol}}^{\text{ADP-Pi}} = \frac{1}{\frac{k_{\text{off}}^{\text{ADP-Pi}}}{k_{\text{r}}^{\text{BE}} + k_{\text{off}}^{\text{ADP-Pi}}} \cdot \frac{1}{k_{\text{r}}^{\text{BE}} + k_{\text{off}}^{\text{ADP-Pi}}} + \frac{k_{\text{r}}^{\text{BE}}}{k_{\text{r}}^{\text{BE}} + k_{\text{off}}^{\text{ADP-Pi}}} \cdot \left(\frac{1}{k_{\text{r}}^{\text{BE}} + k_{\text{off}}^{\text{ADP-Pi}}} + \frac{1}{k_{\text{off}}^{\text{ADP}}} \right)} = \frac{(k_{\text{off}}^{\text{ADP-Pi}} + k_{\text{r}}^{\text{BE}})k_{\text{off}}^{\text{ADP}}}{k_{\text{off}}^{\text{ADP}} + k_{\text{r}}^{\text{BE}}}. \quad (2)$$

ADP-subunits that reach the barbed end dissociate directly with the rate $k_{\text{off}}^{\text{ADP}}$, giving rise to a depolymerization velocity $v_{\text{depol}}^{\text{ADP}}$. Consequently, the average depolymerization velocity is given by

$$v_{\text{depol}}(t) = \mathcal{P}_1(t)v_{\text{depol}}^{\text{ADP-Pi}} + (1 - \mathcal{P}_1(t))v_{\text{depol}}^{\text{ADP}}, \quad (3)$$

where $\mathcal{P}_1(t)$ and $(1 - \mathcal{P}_1(t))$ are the probabilities that the terminal subunit is in the ADP-Pi- and ADP-state, respectively. As phosphate release on the barbed end is not considered explicitly, but via the effective depolymerization velocity $v_{\text{depol}}^{\text{ADP-Pi}}$, the time evolution of the probability $\mathcal{P}_1(t)$ is governed by

$$\frac{\partial \mathcal{P}_1(t)}{\partial t} = -v_{\text{depol}}^{\text{ADP-Pi}}\mathcal{P}_1(t)(1 - \mathcal{P}_2(t)) + v_{\text{depol}}^{\text{ADP}}(1 - \mathcal{P}_1(t))\mathcal{P}_2(t), \quad (4)$$

where $\mathcal{P}_2(t)$ is the probability that the penultimate subunit is in the ADP-Pi-state. The first term on the r.h.s. of the equation accounts for the depolymerization of an ADP-Pi-subunit (both direct dissociation and phosphate release followed by dissociation of an ADP-subunit, see equation 2) and an ADP-subunit on the penultimate position. The second term accounts for the opposite situation: Dissociation of an ADP-subunit followed by an ADP-Pi-subunit.

During fast elongation, a cap of ATP-actin is present at the growing barbed end. This cap prevents the exposure of ADP-Pi-subunits to the barbed end which would result in enhanced phosphate release, cf. section IV. Thus the probability for the penultimate subunit to be in the ADP-Pi-state decays exponentially with its age τ , i.e. the time since it has been incorporated into the filament:

$$\mathcal{P}_2(t) = e^{-k_{\text{r}}\tau}, \quad (5)$$

Filaments elongated with a constant velocity v_{pol} during the polymerization phase. Thus the age of a subunit is a linear function of its position within the filament. Moreover, during depolymerization, the penultimate subunit comoves with the tip of the filament. Thus the age of the penultimate subunit is a function of both the filament length $L(t)$ and the time t since the initiation of depolymerization, cf. fig. 1g in the main text:

$$\tau(t, L) = t + \tau_{\text{pol}} - L(t)/v_{\text{pol}}, \quad (6)$$

where τ_{pol} is the known duration of polymerization. In consequence, the differential equation

$$\frac{\partial \mathcal{P}_1(t)}{\partial t} = -v_{\text{depol}}^{\text{ADP-Pi}} \mathcal{P}_1(t) - (v_{\text{depol}}^{\text{ADP}} - v_{\text{depol}}^{\text{ADP-Pi}}) \mathcal{P}_1(t) e^{-k_r \tau(t,L)} + v_{\text{depol}}^{\text{ADP}} e^{-k_r \tau(t,L)}, \quad (7)$$

with the initial condition

$$\mathcal{P}_1(0) = 1, \quad (8)$$

determines $\mathcal{P}_1(t)$ and via equation 3 the depolymerization velocity. This leads to a second order differential equation for $L(t)$ which describes the depolymerization dynamics. Since phosphate release within the filament is much slower than dissociation, the asymptotic approximation

$$\frac{\partial \mathcal{P}_1(t)}{\partial t} / v_{\text{depol}}^{\text{ADP-Pi}} \approx 0 \quad (9)$$

can be employed, leading to

$$\mathcal{P}_1(\tau) \approx \frac{v_{\text{depol}}^{\text{ADP}} e^{-k_r \tau}}{(v_{\text{depol}}^{\text{ADP}} - v_{\text{depol}}^{\text{ADP-Pi}}) e^{-k_r \tau} + v_{\text{depol}}^{\text{ADP-Pi}}}. \quad (10)$$

With eq. 3, we derive equation (1) of the main text as an asymptotic approximation for the depolymerization velocity in the case of random phosphate release:

$$\frac{1}{v_{\text{depol}}(\tau)} \approx \frac{1}{v_{\text{depol}}^{\text{ADP}}} + \left(\frac{1}{v_{\text{depol}}^{\text{ADP-Pi}}} - \frac{1}{v_{\text{depol}}^{\text{ADP}}} \right) e^{-k_r \tau}. \quad (11)$$

The experimental data are given as length vs time curves. Thus, for the purpose of data analysis, it is most suitable to reformulate this relation for $v(\tau)$ as a differential equation for $L(t)$:

$$\frac{\partial L(t)}{\partial t} \approx \frac{-1}{\frac{1}{v_{\text{depol}}^{\text{ADP}}} + \left(\frac{1}{v_{\text{depol}}^{\text{ADP-Pi}}} - \frac{1}{v_{\text{depol}}^{\text{ADP}}} \right) e^{-k_r \tau(t,L)}}. \quad (12)$$

Partial derivatives with respect to the parameters can be calculated in order to fit the resulting curve to the experimental data, cf. section III.

B. Vectorial phosphate release

In the vectorial model, the phosphate can only be released from a ADP-Pi-subunit adjacent to an ADP-subunit. Thus there is an interface between a segment of ADP-subunits at the pointed end side and another segment of ADP-Pi-subunits at the barbed end side, cf. fig. 1a of the main text. This interface moves with a velocity given by

the release rate k_r towards the barbed end. Meanwhile, the barbed end moves with the depolymerization velocity of ADP-Pi-subunits $v_{\text{depol}}^{\text{ADP-Pi}}$ in the opposite direction. When the interface reaches the barbed end, it vanishes and the filament continues to shrink with the depolymerization velocity $v_{\text{depol}}^{\text{ADP}}$ of ADP-subunits. Thus the function $L(t)$ exhibits a kink when the interface reaches the end at time τ_1 :

$$L(t) = \begin{cases} L_0 - v_{\text{depol}}^{\text{ADP-Pi}}t & \text{for } t \leq \tau_1 \\ L_0 + (v_{\text{depol}}^{\text{ADP}} - v_{\text{depol}}^{\text{ADP-Pi}})\tau_1 - v_{\text{depol}}^{\text{ADP}}t & \text{for } t > \tau_1. \end{cases} \quad (13)$$

Note that the ensemble average exhibits a smooth transition from slope $v_{\text{depol}}^{\text{ADP-Pi}}$ to $v_{\text{depol}}^{\text{ADP}}$ as the period τ_1 can slightly vary within the filament ensemble. However, the distribution of τ_1 within the filament population is very narrow. It will become clear in the next section that the vectorial model does not fit the data.

To be experimentally detectable, the rate of phosphate release of the ADP-Pi-subunit at the interface must be of the same order as the dissociation rate. However, equation (1) in the main text still holds, since there is no change in the ADP-Pi content within the distinct segments.

III. DATA ANALYSIS OF FILAMENT LENGTHS

A. Vectorial vs random mechanism

In this section, we formally check that the depolymerization velocity is continuously increasing from $v_{\text{depol}}^{\text{ADP-Pi}}$ to $v_{\text{depol}}^{\text{ADP}}$, consistent with the random mechanism of phosphate release, rather than suddenly changing from $v_{\text{depol}}^{\text{ADP-Pi}}$ to $v_{\text{depol}}^{\text{ADP}}$, as predicted by the vectorial mechanism. We do this without transforming the original $L(t)$ into $v(\tau)$ data. Thus we fit both a piecewise-linear function as prescribed by the vectorial model and $L(t)$ as given by equation 12 of the random model to the experimental data. The sum of squared residuals SSR provides a relative measure to compare the quality of both fits. With an average of $SSR_{\text{random}} = 9.3 \times 10^4$, compared to $SSR_{\text{vectorial}} = 1.25 \times 10^5$, we find that the model of random phosphate release describes the data better, consistent with the continuous course of $v(\tau)$.

It follows from a theoretical analysis of the vectorial model that the times τ_1 when the putative interface between ADP-Pi- and ADP-subunits reaches the barbed end are almost identical within the filament populations. However, fitting the data from each filament with a piecewise linear function leads to a broad τ_1 distribution, indicating another inconsistency of the data with the vectorial model.

B. Numerical values of kinetic parameters

In this section, we fit the $L(t)$ curve of the random model, given by equation 12, to the experimental data. In the fitting procedure, the known values of τ_{pol} and v_{pol} are fixed to determine the three unknown parameters $v_{\text{depol}}^{\text{ADP-Pi}}$,

$v_{\text{depol}}^{\text{ADP}}$, and k_r . This fitting approach is intended as a comparison for the method described in the main text, i.e. conversion of $L(t)$ curves into $1/v(\tau)$ curves and fitting them with an exponential.

We proceed in two different ways. First, we fit individual curves to each of the $N = 20$ filaments, cf. inset of Fig. S5, to obtain a set of $N = 20$ numerical values for each parameter. The means and standard deviations are given by $v_{\text{depol}}^{\text{ADP}} = (6.3 \pm 1.5)$ subunits/s, $v_{\text{depol}}^{\text{ADP-Pi}} = (1.7 \pm 0.7)$ subunits/s and $k_r = (0.0083 \pm 0.0043)$ /s. These results are in agreement with the values determined in the main text.

The other option for an analysis is to fit a single curve simultaneously to the data from all filaments. This gives the best estimate for the parameters. However, the $N = 20$ data sets were not obtained from a single, but 5 individual experiments whose τ_{pol} and v_{pol} differ. Thus only the filament data within one experiment can be fitted simultaneously, cf. Fig. S5.

We obtain the following values for the weighted total averages of the parameters: $v_{\text{depol}}^{\text{ADP}} = 6.0$ subunits/s, $v_{\text{depol}}^{\text{ADP-Pi}} = 1.5$ subunits/s and $k_r = 0.0074$ /s, in agreement with both the values determined before and the values determined with the method described in the main text. Equation 2 can be restated as

$$k_r^{\text{BE}} = \frac{(v_{\text{depol}}^{\text{ADP-Pi}} - k_{\text{off}}^{\text{ADP-Pi}})k_{\text{off}}^{\text{ADP}}}{k_{\text{off}}^{\text{ADP}} - v_{\text{depol}}^{\text{ADP-Pi}}}, \quad (14)$$

and with $k_{\text{off}}^{\text{ADP-Pi}} = 0.16$ /s and $k_{\text{off}}^{\text{ADP}} = 5.8$ /s, as given in the main text, we obtain $k_r^{\text{BE}} = 1.8$.

IV. SIMULATIONS

In the analytical calculations for the random release mechanism which finally led to equation 12, or equivalently equation (1) in the main text, the following simplifications were made .

- It was assumed that ATP-actin has a infinitely short lifetime within the filament. This is justified by the largeness of the known cleavage rate $k_c = 0.3$ /s [ref 17 in the main text] compared to the release rate k_r .
- Phosphate release at the barbed end does not take place during polymerization. Even though we neglect ATP-actin-subunits in terms of hydrolysis, we assume that a cap of ATP-actin is present during polymerization which prevents ADP-Pi-subunits from losing their phosphate by being exposed at the barbed end. This assumption is justified by the smallness of the cleavage rate $k_c = 0.3$ /s compared to the association rates in the experiment which are typically larger than 10/s.
- When considering the departure of an ADP-Pi-subunit, we do not distinguish between the two possible routes (cf. fig. 3 of the main text), but use an effective depolymerization rate $v_{\text{depol}}^{\text{ADP-Pi}}$ given by 2. However this can only lead to errors on the scale of single subunits.
- As discussed in the main text, the phosphate release rate k_r is much smaller than the dissociation rates $k_{\text{off}}^{\text{ADP-Pi}}$ and $k_{\text{off}}^{\text{ADP}}$. Thus we assume that $\mathcal{P}_1(t)$ is constant on depolymerization time scales.

In order to validate these simplifications, we use the Gillespie algorithm [1] which gives exact stochastic trajectories, to simulate the polymerization and depolymerization of filaments.

The following stochastic processes, which are known to play a role in actin dynamics, are taken into account. ATP cleavage with the rate $k_c = 0.3/s$ [ref. 17 in the main text]; phosphate release with the rate $k_r = 0.0074/s$; enhanced phosphate release at the barbed end with the rate $k_r^{BE} = 1.8/s$; association of ATP-actin with the rate $k_{on}^{ATP} = 15/s$ (only during polymerization phase which lasted for $\tau_{pol} = 300/s$); dissociation of ATP-actin with the rate $k_{off}^{ATP} = 1.4/s$ [ref. 21 in the main text]; dissociation of ADP-Pi-actin with the rate $k_{off}^{ADP-Pi} = 0.16/s$; and dissociation of ADP-actin with the rate $k_{off}^{ADP} = 6/s$. Apart from k_c and k_{off}^{ADP} , the numerical values for the rates were taken from the last section.

It is shown in Fig. S7, that the simulations indeed justify the simplifications which were made to obtain the analytical results, and especially equation (1) in the main text. The irrelevance of the ATP-subunits as an intermediate during depolymerization and its importance during polymerization as a protective cap against enhanced phosphate release becomes clear with Fig. S6. The simulations also indicate the length fluctuations which follow from the stochasticity of the involved transitions. During the first instances of growth, the polymerization trajectories tend to diverge, leading to a spreading in the length at the beginning of depolymerization. During the depolymerization process, this spread varies only slightly.

[1] D. T. Gillespie, *Journal of Physical Chemistry* **81**, 2340 (1977).

Supporting Information

Figure S1 Comparison of depolymerization traces from different individual filaments, under different conditions. Filaments were depolymerized in F buffer after elongation from (A) MgATP actin or (B) MgADP actin. Filaments were depolymerized (C) in the presence of 20 μM profilin after elongation from MgATP actin, or (D) in the presence of 40 μM profilin after elongation from MgADP actin. Some traces have been shifted vertically in order to ease their comparison. For each filament, the depolymerization trace terminates when the filament becomes too short to be reliably measured, when it fragments, or when it pauses. Pauses (indicated here by a dotted line) are discarded during data analysis. (PDF)

Figure S2 Pauses occurring during depolymerization are unrelated to the acceleration of depolymerization, which reflects the ADP Pi content of the filament. Left: Length versus time for a filament depolymerizing with 80 μM profilin. Depolymerization is interrupted by a pause between 100 and 150 s after the beginning of depolymerization. Right: $1/v_{\text{depol}}$ versus the age of F actin, for the same filament, excluding the pause (blue diamonds) and exponential fit (black line). (PDF)

Figure S3 Depolymerization of an ADP actin filament obtained by aging. A filament grown with 2 μM MgATP actin is then left to age at constant length in the presence of 0.1 μM actin (steady state concentration for the barbed end) for 6 min, before initiating depolymerization at time $t = 0$. (PDF)

Figure S4 The length of the ADP Pi F actin at growing barbed ends depends on the age of filaments. Filaments growing in coherent fashion in the presence of 3 μM G actin (50% pyrene labeled) and the indicated amounts of spectrin actin seeds (s.a.s.) were depolymerized by 6 fold dilution in F buffer in the presence of 5 μM Latrunculin A as soon as 20% of actin was assembled. Time courses of growth (left) and depolymerization (right), with the first 100 s of smoothed depolymerization curves presented on the inset. The lag time is visible, and it is longer for younger filaments. (PDF)

Figure S5 Direct fit of depolymerization curve to experimental data. The theoretical curve, given by the differential equation 12 of the supporting text, is fitted to the depolymerization curves of six filaments from one experiment. These curves were slightly shifted in a vertical direction to have a common initial length. Inset: The theoretical curve is fitted to a single experimental curve. (PDF)

Figure S6 Simulation of the length during polymerization and depolymerization. The rates are specified in the Text S1. Top: A cap of ATP actin is present during polymerization, but not during depolymerization. Number of ATP subunits (red), ADP Pi subunits (black), ADP subunits (green), and overall number (blue). Bottom: Fluctuations indicated by 20 randomly chosen trajectories. (PDF)

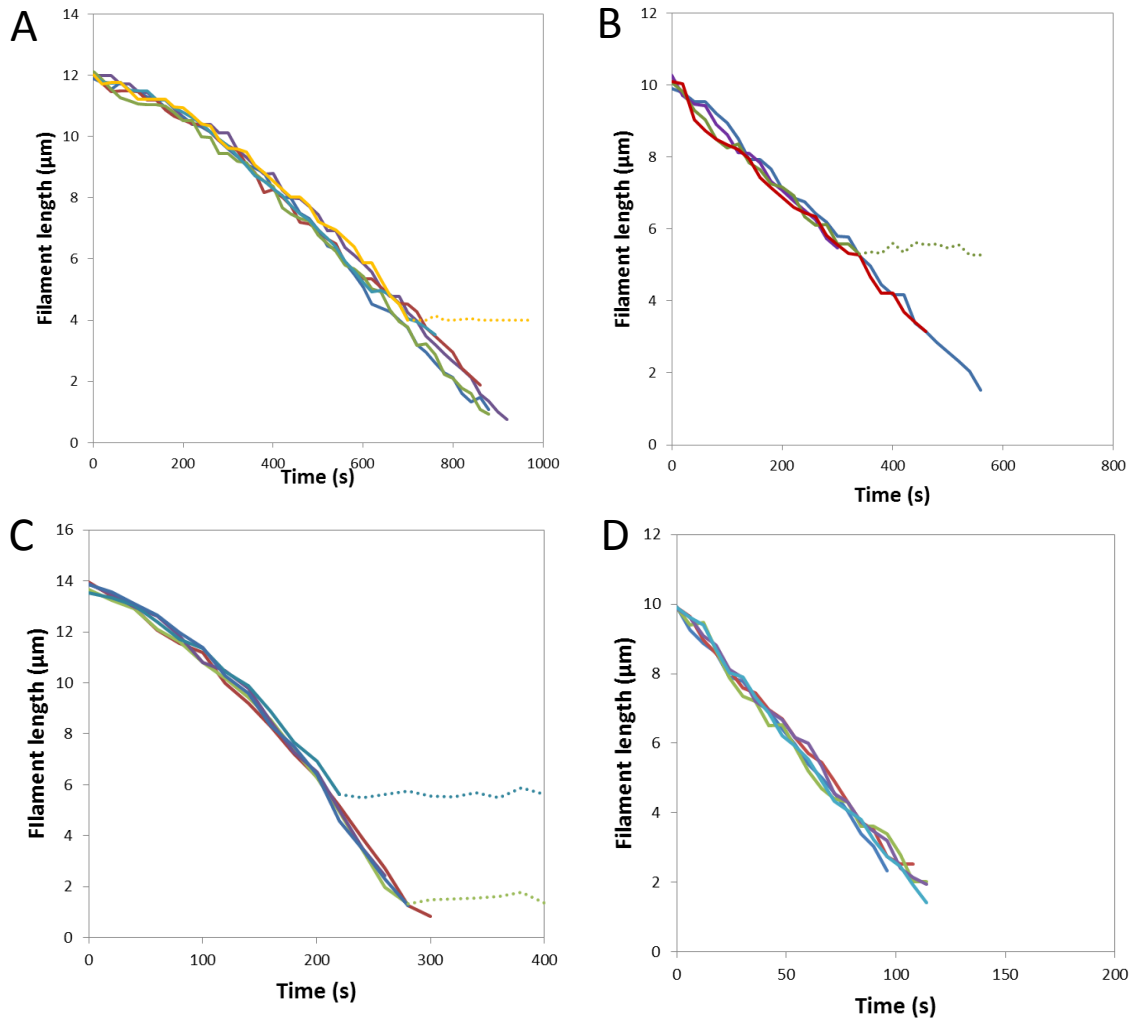
Figure S7 Comparison of simulations with analytical results. We simulated the polymerization and depolymerization of 10,000

filaments with rates as specified in Text S1, i.e. including ATP cleavage. Average values (blue dots) \pm standard deviations (blue dashed lines) are depicted. The continuous red line is the solution of equation 12 of Text S1 for the same parameters as used in the simulations. The fit is sufficient, since the deviation is much smaller than the optical resolution. The small error is mainly caused by neglecting the cleavage step. In a further improved approximation, we could consider ATP cleavage by an effective release rate which takes both cleavage and release into account. Thus we replace k_r by $k_r k_c / (k_r + k_c)$ in equation 12 of the Text S1. This yields the green line, which is in very good agreement with the simulations. Inset: The exponential relation between $1/v(\tau)$ $1/k_{\text{off}}^{\text{ADP}}$ and $\tau = t + t_{\text{pol}} L(t)/v_{\text{pol}}$ is also found for simulated trajectories. The agreement with the analytical results shows that fitting the experimental $1/v(\tau)$ curves with an exponential indeed reveals the correct parameters. (PDF)

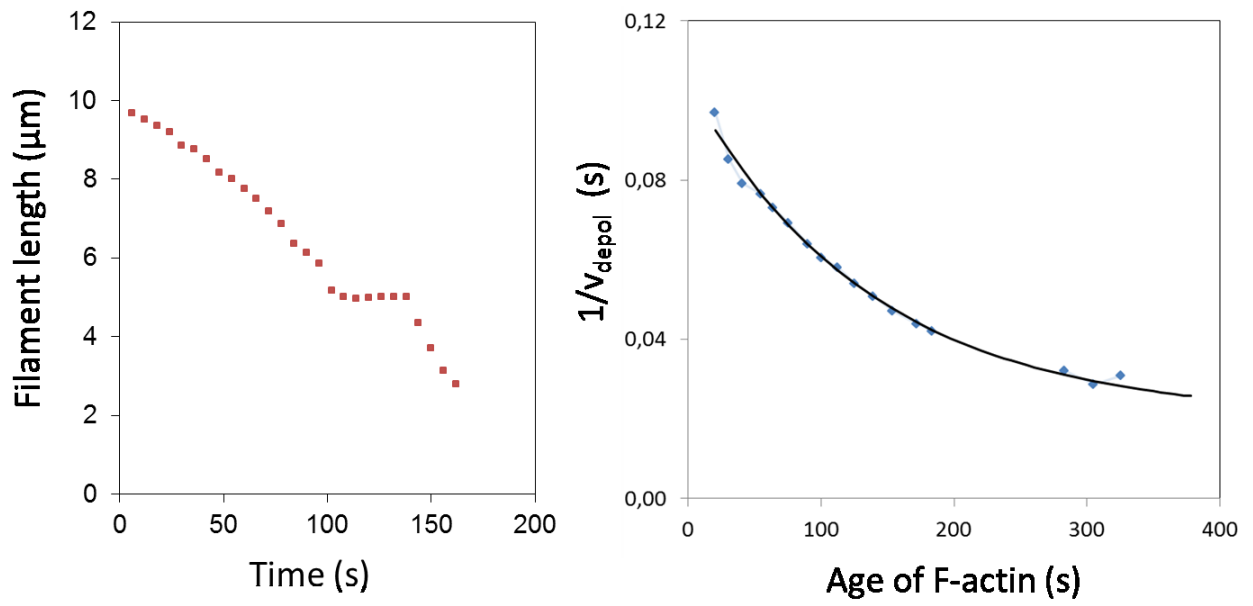
Figure S8 The depolymerization of ADP actin filaments slows down upon exposure to Pi. A filament elongated from MgADP actin was depolymerized in standard F buffer for 60 s (blue diamonds) then in the presence of 25 mM Pi (red squares). Lines represent linear fits of the data. At this resolution, the transition to a slow depolymerization rate appears instantaneous upon exposure to Pi, as expected from the rapid Pi association to the barbed end reported by Fujiwara et al. [25]. In the presence of 25 mM Pi, ADP actin filaments depolymerized at a rate of 0.64 ± 16 subunits/s, which is also in agreement with the values reported in [25]. (PDF)

Figure S9 The effect of profilin during depolymerization is fully reversible. A depolymerizing filament is exposed to 100 μM profilin for 1 min and subsequently switched back to depolymerization in buffer without profilin. (PDF)

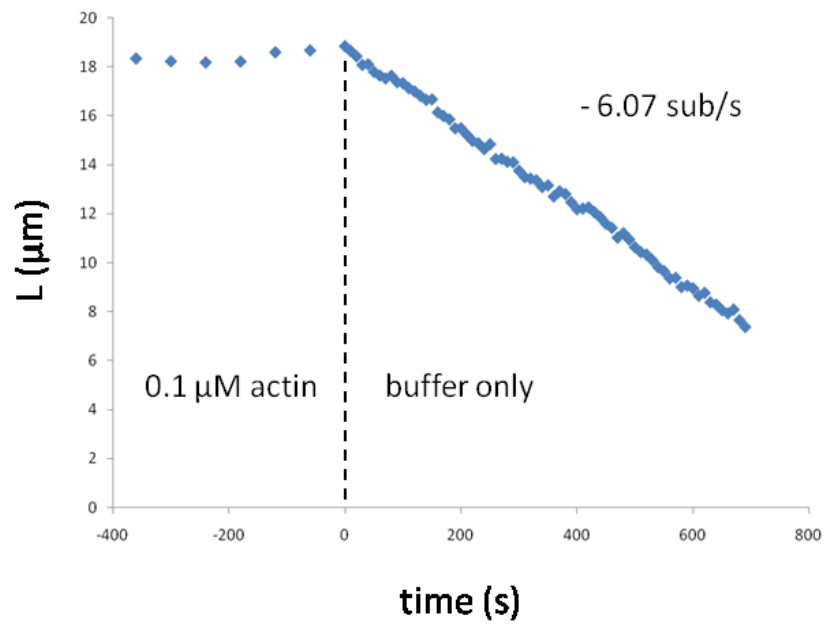
Figure S10 Filaments do not elongate from MgADP G actin in the presence of profilin. (A) Barbed end and pointed end growths from 16.4 μM (blue) and 10.5 μM (red) MgADP G actin (2% pyrene labeled) were initiated using 0.2 nM spectrin actin seeds (open circles) or 10 nM gelsolin actin seeds (closed squares), respectively, in the presence of the indicated amounts of profilin. The extent of F actin assembled at equilibrium (reached in less than 1 h) was measured. Identical linear decrease in F ADP actin with capped and non capped filaments shows that profilin binds MgADP G actin with $K_d = 2.1 \mu\text{M}$ (this value was confirmed by measurements of tryptophan fluorescence quenching upon binding of profilin to actin unpublished data) and that profilin MgADP G actin does not productively associate with barbed nor pointed ends. Profilin MgADP G actin hence accumulates in solution as described by $[PA] = [P]_0 A_c / (A_c + K_d)$, where $[P]_0$ is the total profilin concentration and A_c is the critical concentration for ADP G actin assembly at either barbed or pointed ends. In contrast, in Kinosian et al.'s view [33] the proposed productive association of profilin MgADP G actin at barbed ends specifically would have led to a steeper decrease of F actin concentration for capped filaments than for non capped filaments in ADP, like the observed behavior in ATP. (B) Elongation rate of MgADP actin filaments, in the presence of 5 μM MgADP G actin and the indicated amounts of profilin, measured on individual filaments in a microflow. (PDF)



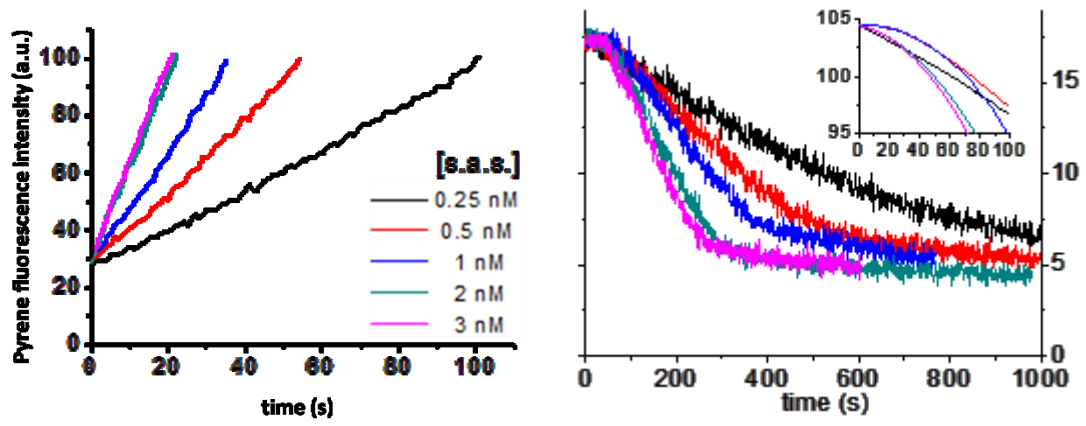
Jégou et al. Figure S1.



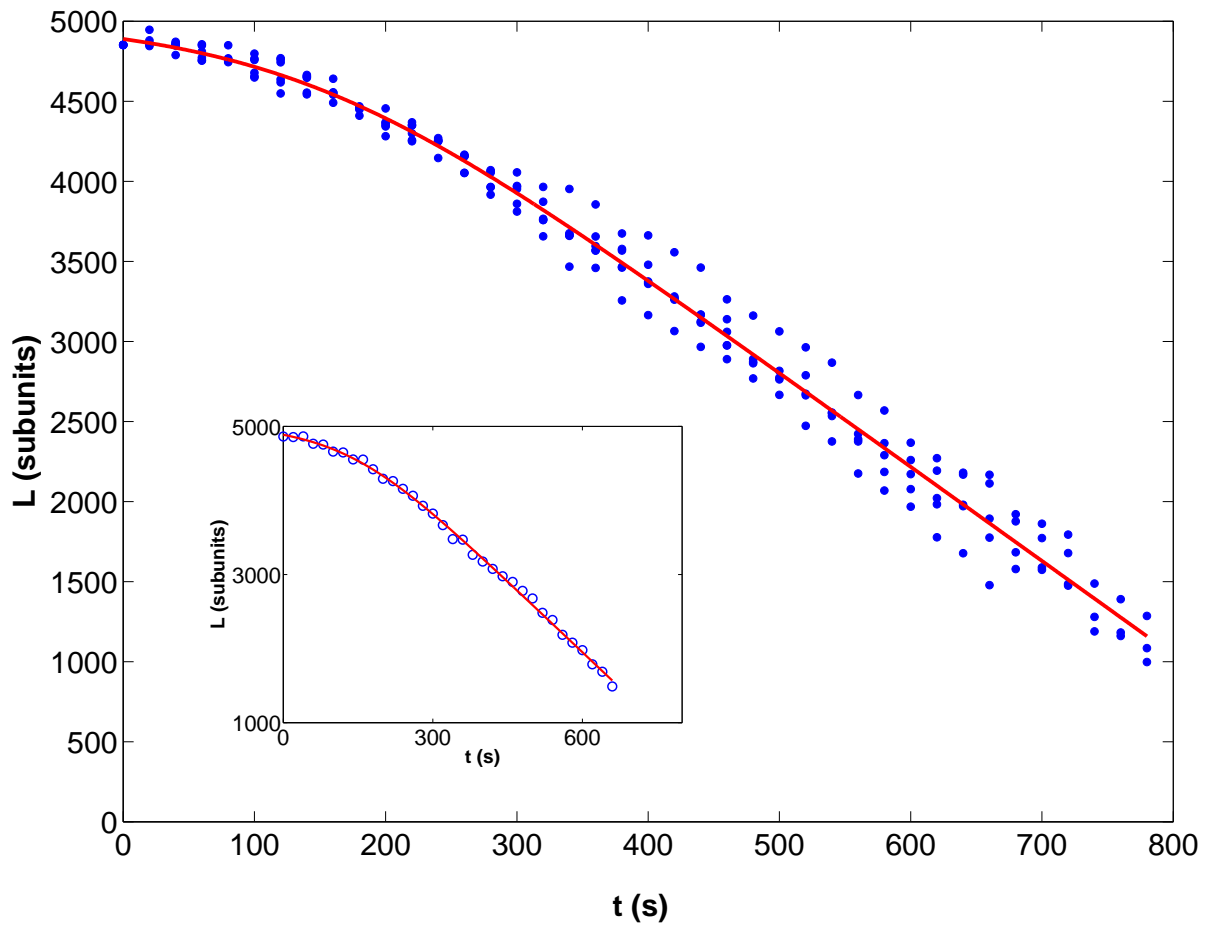
Jégou et al. Figure S2



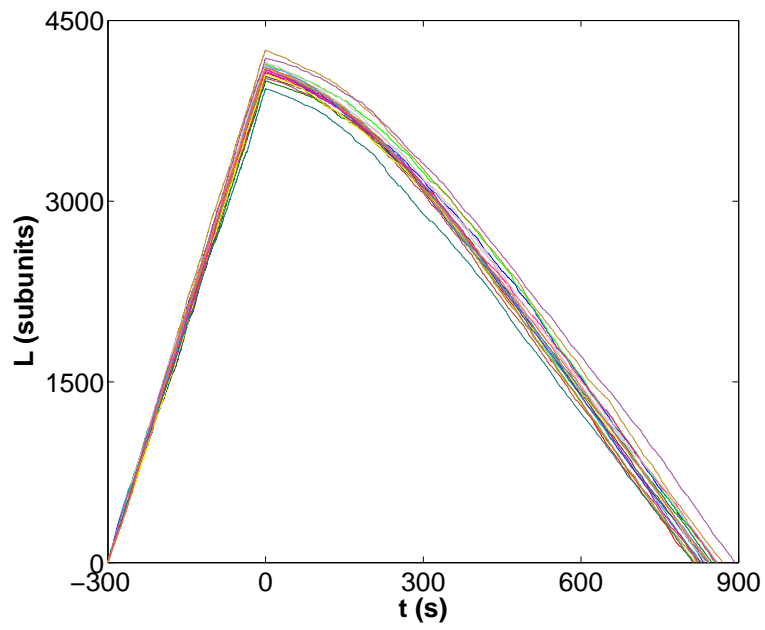
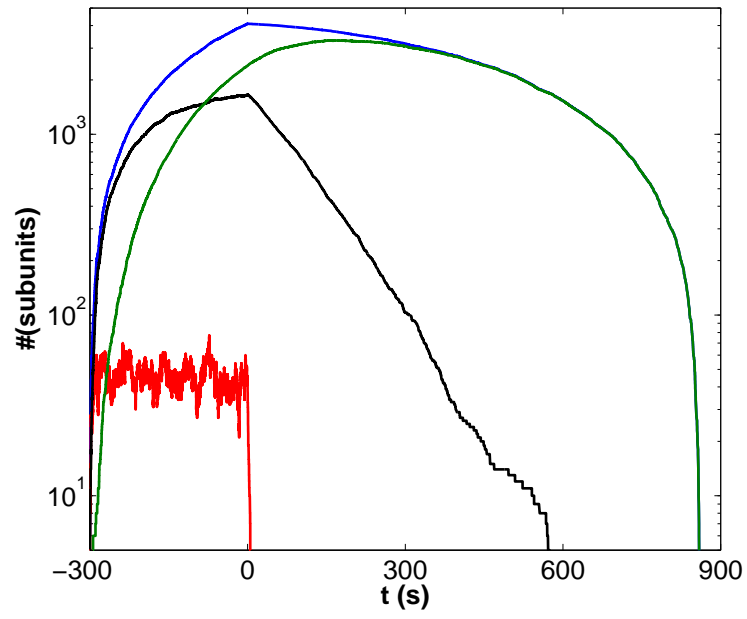
Jégou et al. Figure S3



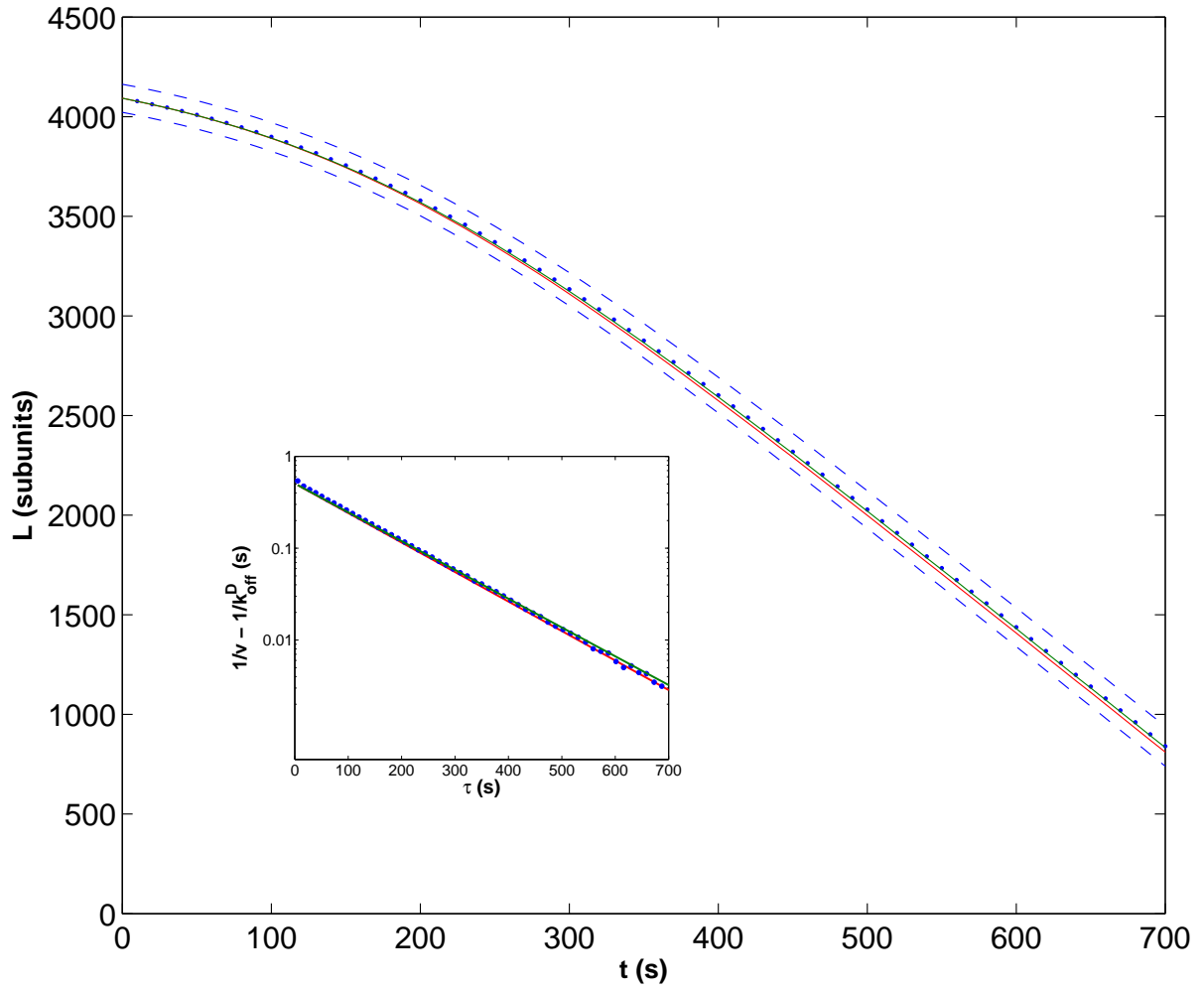
Jégou et al. Figure S4



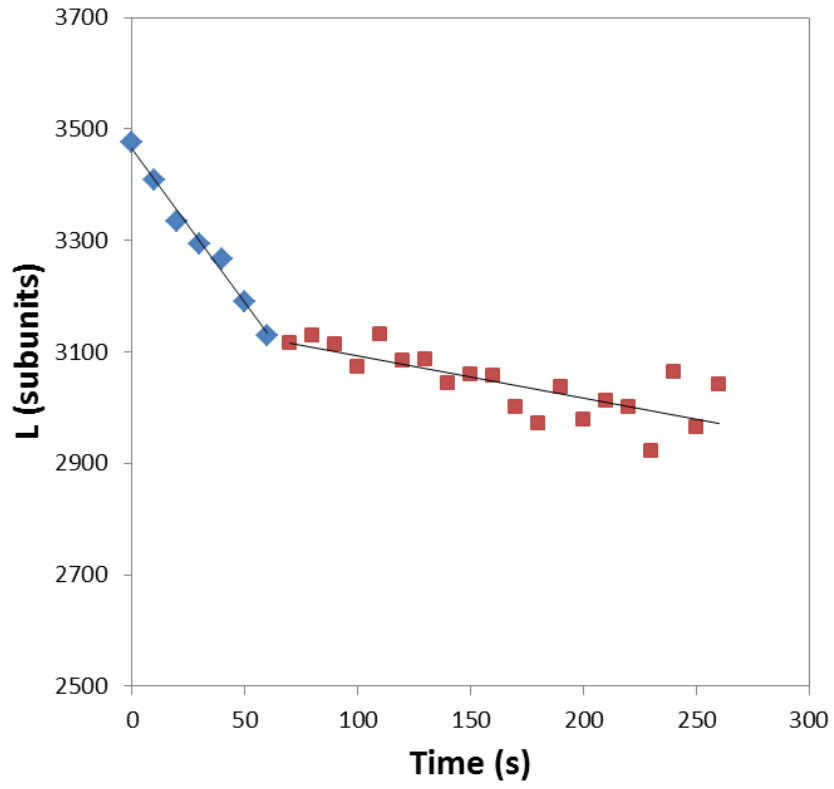
Jégou et al. Figure S5



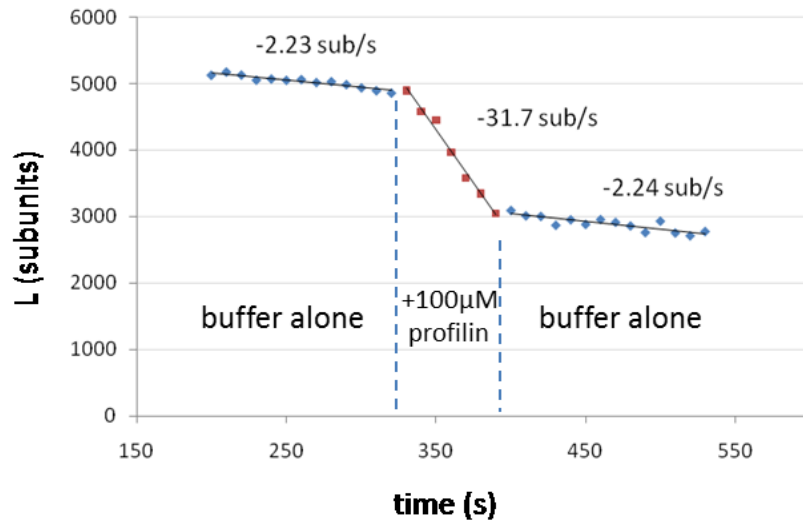
Jégou et al. Figure S6



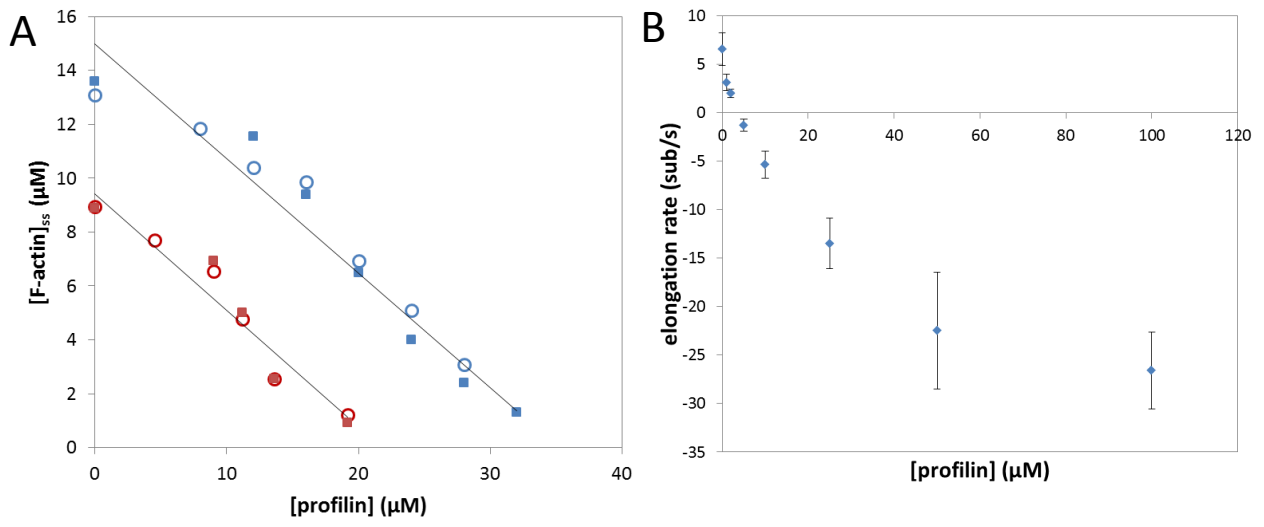
Jégou et al. Figure S7



Jégou et al. Figure S8



Jégou et al. Figure S9



Jégou et al. Figure S10